*American Mineralogist, Volume 67, pages 1218–1228, 1982*

# Andalusite–kanonaite series: lattice and optical parameters

MICKEY GUNTER AND F. D. BLOSS

*Department of Geological Sciences*
*Virginia Polytechnic Institute and State University*
*Blacksburg, Virginia 24061*

**Abstract**

For 20 crystals ranging compositionally between pure andalusite ($Al_2SiO_5$) and 62 mole percent kanonaite ($MnAlSiO_5$), some containing $Fe^{3+}$, cell edges *a*, *b*, and *c* were determined by back-reflection Weissenberg techniques, refractive indices for sodium light vibrating parallel to **a**, **b**, and **c** (symbols: $n_a$, $n_b$, and $n_c$) were determined (to ±0.0005) by spindle stage methods, and the values for *x* and *y* in the general formula $Al_{1-x-y}Mn^{3+}_xFe^{3+}_yAlSiO_5$ were determined from electron microprobe analyses. Multiple linear regressions disclosed that cell edges *a* and *b* increased more with *x* than with *y* but that *c* increased with *y* but hardly at all with *x*. These changes are inferred to result primarily from dimensional changes in the M(1) octahedra if occupied by $Mn^{3+}$ (Jahn–Teller distortion and elongation of the M(1)–O(4) distance) or by $Fe^{3+}$ (enlargement without such distortion).

Substitution of $Fe^{3+}$ increases $n_a$, $n_b$ and $n_c$ significantly more than does $Mn^{3+}$. Thus the standard plots of index *versus* $[x + y]$ can only approximately conform to the data. Regressions indicate that $n_a$, $n_b$ and $n_c$ are non-linearly related to $[x + y]$. Surprisingly, the resultant curves all intersect at or near a common point and near-isotropic andalusites may exist near $[x + y]$ equal 0.066. The curve intersections explain the differences in optic orientation between andalusites ($c = X$) and kanonaites and viridines ($c = Z$). Relative to the {110} cleavage, therefore, andalusite is characterized by (−) elongation whereas kanonaites and viridines possess (+) elongation.

Regressions performed on the data for 11 specimens (= andalusites) for which $[x + y] < 0.05$ predict the following properties for pure andalusite: $a = 7.7923(3)$, $b = 7.8965(2)$, $c = 5.5534(4)$Å, $D$(calc) = 3.149 g/cm$^3$, molar volume = 51.45(4) cm$^3$ and (for 589.3 nm) the indices 1.6328(3), 1.6386(2) and 1.6436(4) with $2V$(calc) = −85.5°. The indices most commonly cited by modern textbooks—1.629, 1.633 and 1.638—are for a (+) crystal whereas andalusite is (−). Ironically, they overlook those reported by Taubert (1905), namely, 1.6326, 1.6390 and 1.6440.

## Introduction

The polymorphs of $Al_2SiO_5$—namely, andalusite, sillimanite, and kyanite—have long been studied for use as geothermometers and geobarometers in metamorphic petrology. Despite such intensive study, the location of the triple point for these three polymorphs remains moot. As reasons for the discrepancies, Holdaway (1971, p. 98) cites: (1) the difficulties encountered in determining reliable equilibrium data for most silicate systems at moderately low temperatures and pressures and (2) the possibility that deviations from the ideal composition $Al_2SiO_5$ might affect the relative stabilities of the polymorphs. Holdaway discounts factor (2), however, concluding that "the only elements present in more than trace amounts in one or more of the polymorphs are $Fe^{3+}$ and $Mn^{3+}$," and that the solid solution of $Fe^{3+}$ in $Al_2SiO_5$ polymorphs does not importantly affect their relative stabilities "except, to a small extent, in the andalusite–sillimanite boundary." By contrast, Strens (1968, p. 846) had earlier concluded that high Mn content might stabilize andalusite into the field of sillimanite and kyanite.

Some andalusites may be rich in $Mn^{3+}$ and, often, in $Fe^{3+}$ as well. The extent to which this affects the field of stability of andalusite remains moot. However, the possibility of this has increased interest in the effects of $Mn^{3+}$ and $Fe^{3+}$ substitution upon the cell dimensions and optical properties of andalusite. Thus, Herbosch (1968), Vrana *et al.* (1978), and

0003–004X/82/1112–1218$02.00

Abs-Wurmbach *et al.* (1981) have all completed such studies, but none used spindle stage techniques. These techniques, described in detail by Bloss (1981), confer two major advantages: (1) Greater routine precision than heretofore so that principal indices can be determined to ±0.0005 instead of ±0.002 (or ±0.003); and (2) the equally great advantage that one can measure, *from the same single crystal:* $2V$, all principal indices, its lattice parameters, and its composition (by microprobe analysis). These twin advantages permitted new insights into the crystal chemistry of the andalusite–kanonaite series and particularly into the relationship to composition of its refractive indices for light vibrating along the *a, b,* and *c* crystallographic axes. A secondary objective of the paper is to demonstrate the advantage of spindle stage methods for systematic optical studies in combination with crystallographic and chemical measurements.

### *Structure*

The structure (Fig. 1) of andalusite ($Al_2SiO_5$; *Pnnm;* $a = 7.89$, $b = 7.90$, $c = 5.55$Å)—solved by Taylor (1929), refined by Burnham and Buerger (1961), and more recently studied using neutron diffraction by Finger and Prince (1971) and by Peterson and McMullen (1980)—consists of silicate tetrahedra and of Al within distorted M(1) octahedra, and within distorted M(2) trigonal bipyramids. The M(1) octahedra share edges to form continuous chains parallel to the *c* axis. These chains are linked laterally by chains (also parallel to *c*) wherein silicate tetrahedra alternate with M(2) polyhedra.

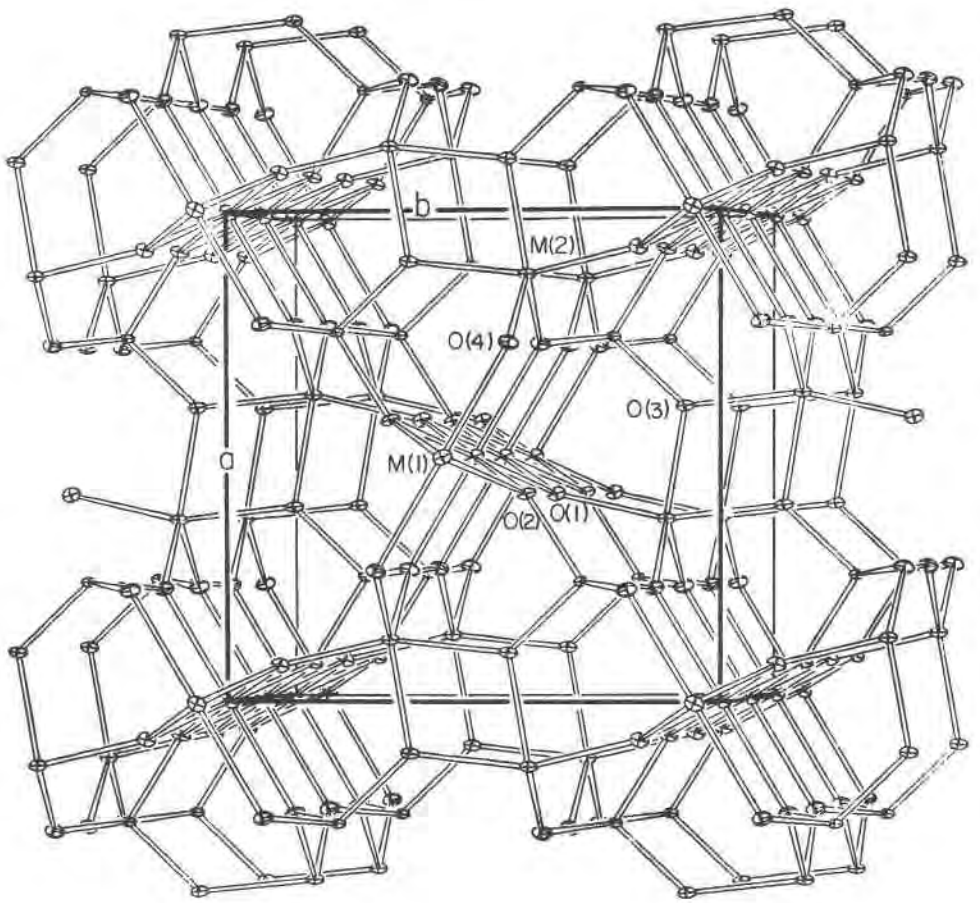


Fig. 1. Ortep drawing of the structure of andalusite. The unit cell is shown with **a** and **b** almost parallel to the page but with **c** (not labelled) almost perpendicular to the page. Site M(1)—6-coordinated at center of a distorted octahedron—and site M(2)—5-coordinated at the center of a distorted bipyramid—are shown relative to oxygens O(1), O(2), O(3), and O(4). Chains of edge-sharing M(1) octahedra run parallel to the *c* axis.

*Formulae and nomenclature*

Vrana *et al.* (1978), on the basis of X-ray data, concluded that the new mineral kanonaite, $(Mn^{3+}_{0.76}Al_{0.23}Fe_{0.02})^{VI}Al^{V}Si^{IV}O_5$, was isostructural with andalusite, $Al^{VI}Al^{V}Si^{IV}O_5$, the Roman numerals here indicating coordination numbers relative to oxygen. They also concluded that $Mn^{3+}$ substituted largely for Al in the octahedral M(1) position. Refinements of kanonaite's structure by Abs-Wurmbach *et al.* (1981) and by Weiss *et al.* (1981) confirmed both conclusions. Thus, Weiss *et al.* obtained refined site occupancies of $Mn_{0.74}Al_{0.26}$ for M(1) and $Mn_{0.12}Al_{0.88}$ for M(2) but recognized that this yields a bulk composition, $Mn_{0.86}Al_{1.14}$, which differs slightly from that from the chemical analysis. Concurrently, Abs-Wurmbach *et al.* (1981), who refined the structures of kanonaite and three other natural andalusites containing significant $Mn^{3+}$ and $Fe^{3+}$, also concluded that $Mn^{3+}$ and $Fe^{3+}$ almost exclusively occupy the M(1) site. The Mössbauer spectra they obtained confirmed this and indicated that only 10 to 15% of the total iron occupied the M(2) site. Consequently, we may write andalusite's general formula as

$$(Al_{1-x-y}Mn^{3+}_{x}Fe^{3+}_{y})^{VI}Al^{V}Si^{IV}O_5$$

This formula embodies a simplification that tacitly assumes that $Mn^{3+}$ and $Fe^{3+}$ substitute only into the M(1) sites, which is not quite the case.

Acting upon the proposals by Vrana *et al.* (1978), the IMA Commission on New Minerals and Mineral Names approved the name kanonaite to apply to the theoretical Mn end member $Mn^{VI}Al^{V}Si^{IV}O_5$. For solid solutions between $MnAlSiO_5$ and $Al_2SiO_5$, the Commission recommends, as noted by Abs-Wurmbach *et al.* (1981), the names manganian andalusite ($Mn^{VI} < Al^{VI}$) and aluminous kanonaite ($Mn^{VI} > Al^{VI}$). Concurrently, the Commission voted 10 to 3 to delete the name viridine, which Klemm (1911) had used for a light green andalusite that contained 4.16% $Fe_2O_3$ and 4.77% $Mn_2O_3$. A possible factor in this decision was that some investigators and texts had strayed from Klemm's original use by applying the term viridine to andalusites rich only in $Mn^{3+}$ despite, for these, the precedence of the name *manganandalusite* (Bäckström, 1896). However, correct usage also persisted. For example, Deer, Howie and Zussman (1966, p. 39) state, "A green variety of andalusite, viridine, contains appreciable ferric iron and manganese." A recent proposal (by F.D.B.) for revalidation of the name viridine for its original use received from the Commission 7 votes of approval and 7 of disapproval, thus failing for lack of a ⅔ majority. Consequently, for specimens called viridines in previous publications, we place the name in quotes. According to the Commission's ruling these specimens should now be called *ferrian manganian andalusites*.

## Experimental procedures

*Crystal selection and orientation*

Under a binocular microscope, crystals selected from each of 20 different samples (Table 1) were mounted on a glass fiber. With this fiber affixed to a goniometer head, the crystal could be first studied optically with a Supper spindle stage which was mounted on the stage of a polarizing microscope. The good {110} cleavage of these crystals made it easy to adjust the goniometer arcs until the crystal's *c* axis was parallel to the axis of the goniometer head. The correct arc settings for this could be confirmed (and refined) by setting the microscope stage at its reference azimuth (Bloss, 1981) and, with the crystal immersed in an oil of index close to $\beta$ for the grain, performing a 360° rotation about the S-axis (= spindle axis). If the crystal did not remain extinct between crossed polars during this rotation, the arcs of the goniometer head were adjusted until it did. At the same time, this examination indicated

Table 1. Sample descriptions and localities

| sample | | description and locality |
|---|---|---|
| 1 | (120399)* | massive xls no matrix (Andalusia, Spain) |
| 2 | | cut gem (Minas Gerais, Brazil) |
| 3 | (115171)* | massive xls, micaceous matrix (Brazil) |
| 4 | (M23285)** | cut gem (Minas Gerais, Brazil) |
| 5 | (98355)* | xls w/qtz bio and mus (near Oreville, SD) |
| 6 | (R11162)* | gemmy xls, no matrix (Minas Novas, Brazil) |
| 7 | (14860)* | green cut gem (Minas Gerais, Brazil) |
| 8 | | (Bradshaw Mtns., Yavapia Co., AZ) |
| 9 | (97418)* | xls in massive qtz w/mus (Clark's Valley, Fresno Co., CA) |
| 10 | (134480)* | xls w/pyrophyllite (Lower Hondo Canyon, Taos Co., NM) |
| 11 | (14860)* | black cut gem (Minas Gerais, Brazil) |
| 12 | (127120)* | xls in feldspathic quartzite (Tjatitsvare, Ultevis, Norbotten, Sweden) |
| 13 | | (Laiovall, Sweden) |
| 14 | (113990)* | xls in quartzite (Petaca Dis., NM) |
| 15 | (127121)* | xls in quartzite (Kiowa Mtn., Petaca Dis., Rio Arriba Co., NM) |
| 16 | (114128)* | xls in quartzite (Kiowa Mtn., Petaca Dis., Rio Arriba Co., NM) |
| 17 | | (Vestana, Sweden) |
| 18 | | (Tanzania) |
| 19 | (M18262)*** | (Tjatitsvare, Ultevis, Sweden ?) |
| 20 | | gahnite-Mg-chlorite-coronadite-qtz-schist (Kanona, Zambia) |

* National Museum of Natural History
** Royal Ontario Museum
*** Field Museum of Natural History

that the crystal was indeed (optically) a single crystal.

After the preliminary optical orientation of the crystal, the goniometer head was transferred to a precession camera to refine its orientation and provide an additional check on crystal perfection. Finally, the crystal was photographed with a back-reflection Weissenberg camera (Buerger, 1937) so as to record, using unfiltered Cu radiation, its high-angle $2\theta$ reflections. Several times, these photographs revealed that a crystal, although it had appeared optically homogeneous, was not a single crystal.

*Lattice parameter determinations*

For each crystal, two back-reflection Weissenberg photographs were made, one with $c$ parallel to the dial axis to obtain $hk0$ reflections and a second with the crystal remounted on the goniometer head and re-oriented so that $a$ (or $b$) was parallel to the dial axis so as to yield $0kl$ or $h0l$ reflections. For each photograph the diffraction spots for Cu$K\alpha_1$, Cu$K\alpha_2$, and Cu$K\beta$ were indexed and their corresponding $2\theta$ values were measured. Approximately 50 to 55 $hk0$ reflections plus 35 to 40 $0kl$ or $h0l$ reflections were thus indexed and measured for each crystal. The resultant $2\theta$ values and reflection indices were submitted to the least-squares refinement program of Burnham (1962, 1965) as revised by L. Finger. This corrects for systematic errors from film shrinkage, absorption, and camera eccentricity while calculating the lattice parameters to the fourth decimal place. For two gem-quality andalusites (samples 2 and 7), the cell edges were also determined by powder diffraction using silicon as an internal standard. The cell edges for sample 7 and for a kanonaite crystal (sample 20) were also checked using normal-beam Weissenberg photos. Finally, the $a$ cell edge for silicon was determined by use of the back-reflection Weissenberg camera. The cell edges thus obtained for these crystals confirm those obtained by the more precise back-reflection Weissenberg method (Table 2).

Table 2. Cell parameters measured by three different methods

| sample | powder | Weissenberg | back-reflection |
|---|---|---|---|
| #2 | a=7.797(3) | ----- | 7.7939(3) |
| | b=7.900(3) | ----- | 7.8975(3) |
| | c=5.556(3) | ----- | 5.5549(6) |
| #7 | a=7.799(5) | 7.794 | 7.7945(2) |
| | b=7.900(4) | 7.899 | 7.8997(2) |
| | c=5.555(3) | 5.554 | 5.5554(4) |
| #20 | a=-------- | 7.953 | 7.9521(5) |
| | b=-------- | 8.044 | 8.0422(5) |
| | c=-------- | ----- | 5.6131(7) |
| silicon | a=5.4309(2)** | ----- | 5.4313(7) |

*Numbers in parentheses represent estimated standard deviations in terms of the least units cited.

**Value from National Bureau of Standards

*Optical methods*

After a crystal's perfection had been confirmed by X-ray diffraction, its optical parameters ($2V$ at several wavelengths, principal refractive indices for sodium light, and its pleochroism) were determined. Using the Bloss and Riess (1973) technique, the microscope stage settings that produced crystal extinction between crossed polars were determined at spindle stage settings of 0, 10, 20, . . . , 350 degrees. This was done at wavelengths 400, 666, and 900 nm for andalusite but at wavelengths 500 and 540 nm for the viridines and kanonaite because, outside the 500–540 nm range, these latter crystals became almost opaque. The extinction data for each wavelength were submitted to the computer program EXCALIBR which then calculated, for that wavelength, $2V$ as well as the spindle and microscope stage settings necessary to orient the crystal so that its three principal refractive indices could be measured without appreciable error due to misorientation. Simultaneously the pleochroic color associated with each principal vibration axis then became observable.

Principal refractive indices were measured using the double variation method as described by Louisnathan *et al.* (1978). Approximately 40 to 72 matches between the grain and each of three separate oils were obtained by varying the temperature of the oil and the wavelength of the incoming light. A computer program calculated the oil's refractive index for the temperature of match and then, by a linear regression method, calculated values for the two constants, $a_0$ and $a_1$, in the linearized Sellmeier equation

$$y = a_0 + a_1 x$$

where $y$ equals $(n^2 - 1)^{-1}$ and $x$ equals $\lambda^{-2}$. With $a_0$ and $a_1$ known, the refractive index $n$ could then be calculated for any wavelength of light desired. This method, when tested using glasses whose refractive

indices were known to the fifth decimal place, yielded refractive indices which were within 0.0005 of the glass's known refractive index for any wavelength within the visible range.

## Data and calculations

For the eleven andalusites, eight viridines, and one kanonaite studied (Table 1), Table 3 summarizes compositions and calculated densities, Table 4 unit cell parameters, Table 5 refractive indices and $2V_x$, and Table 6 pleochroism and absorption. The effect of composition on each unit cell or optical parameter was investigated by performing multiple linear regressions on the data with the parameter serving as the dependent variable and with $x$ and $y$ as independent variables. The SAS GLM procedure (Helwig and Council, 1979) proved convenient for this. This procedure also served to evaluate the intercept $\beta_0$ and coefficients $\beta_1$, $\beta_2$ . . . $\beta_n$ in non-linear models that combined $x$ and $y$ into a single variable, thus

$$a = \beta_0 + \beta_1[x + y] + \beta_2 [x + y]^2 \ldots + \beta_n[x + y]^n$$

where, for example, $a$ represents the $a$ cell edge. From this model, the non-significant higher order terms in $[x + y]$ could be eliminated by generating F-statistics which permitted successive evaluations of the null hypothesis that $\beta_n = 0$, then $\beta_{n-1} = 0$, and so on. For example, assume the null hypothesis could not be rejected for $\beta_n$ to $\beta_2$, but could be for $\beta_1$ in the preceding model. If so the terms $[x + y]^n$ down to $[x + y]^2$ could be dropped as non-significant.

Table 3. Chemical compositions and calculated densities

| sample | $SiO_2$ | $Al_2O_3$ | $Mn_2O_3$ | $Fe_2O_3$ | atomic frequency Mn(=x) | atomic frequency Fe(=y) | calculated density |
|---|---|---|---|---|---|---|---|
| 1 | 37.0(5) | 62.8(2) | 0.00 | 0.18(1) | 0.000 | 0.003 | 3.146 |
| 2 | 36.9(1) | 62.7(2) | 0.00 | 0.23(1) | 0.000 | 0.003 | 3.142 |
| 3 | 37.3(4) | 62.4(3) | 0.01(1) | 0.23(5) | 0.000 | 0.003 | 3.147 |
| 4 | 36.8(5) | 62.8(4) | 0.00 | 0.30(1) | 0.000 | 0.006 | 3.148 |
| 5 | 37.1(3) | 62.4(2) | 0.01(1) | 0.40(1) | 0.000 | 0.006 | 3.146 |
| 6 | 36.7(5) | 62.8(1) | 0.00 | 0.46(7) | 0.000 | 0.010 | 3.150 |
| 7 | 37.0(4) | 62.0(7) | 0.28(2) | 0.69(4) | 0.006 | 0.013 | 3.156 |
| 8 | 37.4(2) | 61.4(5) | 0.01(1) | 1.19(3) | 0.000 | 0.023 | 3.153 |
| 9 | 36.5(4) | 62.0(1) | 0.01(1) | 1.31(2) | 0.000 | 0.026 | 3.151 |
| 10 | 36.5(5) | 61.3(4) | 0.04(1) | 2.01(6) | 0.000 | 0.042 | 3.158 |
| 11 | 36.6(3) | 61.2(3) | 1.50(4) | 0.71(1) | 0.032 | 0.013 | 3.172 |
| 12 | 36.8(1) | 59.2(3) | 1.53(1) | 2.38(7) | 0.033 | 0.050 | 3.172 |
| 13 | 36.3(1) | 59.7(3) | 1.20(5) | 2.74(1) | 0.026 | 0.055 | 3.175 |
| 14 | 36.4(1) | 58.3(5) | 2.77(7) | 1.67(7) | 0.060 | 0.034 | 3.176 |
| 15 | 36.6(1) | 58.5(7) | 2.99(9) | 1.75(7) | 0.063 | 0.037 | 3.176 |
| 16 | 36.5(3) | 57.6(9) | 3.65(8) | 1.69(18) | 0.078 | 0.037 | 3.195 |
| 17 | 36.6(3) | 57.8(3) | 4.29(9) | 1.26(3) | 0.090 | 0.027 | 3.181 |
| 18 | 35.9(4) | 55.0(2) | 6.42(21) | 2.48(13) | 0.138 | 0.054 | 3.203 |
| 19 | 35.8(2) | 46.4(8) | 13.56(51) | 3.57(17) | 0.314 | 0.080 | 3.250 |
| 20 | 34.9(1) | 37.7(4) | 25.74(45) | 0.70(9) | 0.622 | 0.015 | 3.313 |

Numbers in parentheses represent estimated standard deviations in terms of the least units cited.

Table 4. Observed cell edges (Å) and volumes (Å$^3$)

| sample | $a$ | $b$ | $c$ | $V$ |
|---|---|---|---|---|
| 1 | 7.7925(2) | 7.8976(2) | 5.5535(4) | 341.77(3) |
| 2 | 7.7939(3) | 7.8975(3) | 5.5549(6) | 341.92(5) |
| 3 | 7.7922(2) | 7.8969(2) | 5.5552(4) | 341.84(3) |
| 4 | 7.7924(2) | 7.8970(2) | 5.5535(3) | 341.74(3) |
| 5 | 7.7932(2) | 7.8975(1) | 5.5547(3) | 341.87(2) |
| 6 | 7.7927(2) | 7.8977(2) | 5.5548(5) | 341.87(5) |
| 7 | 7.7945(2) | 7.8997(2) | 5.5554(4) | 342.07(3) |
| 8 | 7.7944(2) | 7.9001(2) | 5.5570(3) | 342.18(3) |
| 9 | 7.7939(2) | 7.9007(2) | 5.5592(5) | 342.32(4) |
| 10 | 7.7964(2) | 7.9039(2) | 5.5616(5) | 342.71(4) |
| 11 | 7.8021(2) | 7.9055(2) | 5.5576(4) | 342.79(3) |
| 12 | 7.8072(2) | 7.9132(2) | 5.5687(4) | 344.03(3) |
| 13 | 7.8051(2) | 7.9118(2) | 5.5682(3) | 343.84(2) |
| 14 | 7.8101(2) | 7.9145(2) | 5.5667(4) | 344.09(4) |
| 15 | 7.8166(3) | 7.9189(3) | 5.5675(5) | 344.62(5) |
| 16 | 7.8053(4) | 7.9128(4) | 5.5663(6) | 343.79(6) |
| 17 | 7.8207(2) | 7.9222(2) | 5.5685(3) | 345.01(3) |
| 18 | 7.8353(4) | 7.9382(3) | 5.5786(5) | 346.98(5) |
| 19 | 7.8906(3) | 7.9870(3) | 5.5999(4) | 352.92(4) |
| 20 | 7.9521(5) | 8.0422(5) | 5.6131(7) | 358.98(7) |

Numbers in parentheses represent estimated standard deviations in terms of the least units cited.

## Results and discussion

The aforementioned regression procedures, if applied to the data from all 20 crystals, yielded equation-models 1 to 16 (Tables 7, 8). The even-numbered equations treat $[x + y]$ as a single variable and contain higher order terms in $[x + y]$ only if their coefficients proved significant. Equations 1a to 16a resulted from regressions performed on only the data from the 11 andalusites (for which $[x + y] < 0.05$).

Table 5. Refractive indices observed for sodium light, $2V$ calculated from same, and $2V$ determined by Bloss-Riess (1973) method for wave-lengths 400, 666, and 900 nm

| sample | $n_a$ | $n_b$ | $n_c$ | $2V_c$ calc | $2V$ 400 | $2V$ 666 | $2V$ 900 |
|---|---|---|---|---|---|---|---|
| 1 | 1.6439 | 1.6386 | 1.6329 | 87.6 | 86.7 | 84.1 | 86.3 |
| 2 | 1.6439 | 1.6395 | 1.6342 | 84.4 | 85.6 | 83.1 | 82.6 |
| 3 | 1.6448 | 1.6398 | 1.6340 | 85.5 | 85.2 | 84.4 | 82.6 |
| 4 | 1.6444 | 1.6397 | 1.6340 | 84.2 | 85.5 | 84.6 | 85.5 |
| 5 | 1.6446 | 1.6403 | 1.6351 | 84.3 | 83.2 | 83.6 | 83.5 |
| 6 | 1.6446 | 1.6404 | 1.6350 | 82.6 | 84.1 | 83.4 | 81.6 |
| 7 | 1.6460 | 1.6417 | 1.6363 | 83.2 | 86.4 | 85.8 | 84.2 |
| 8 | 1.6458 | 1.6427 | 1.6385 | 81.1 | 80.8 | 81.8 | 83.2 |
| 9 | 1.6490 | 1.6445 | 1.6385 | 81.5 | 81.4 | 82.2 | 81.0 |
| 10 | 1.6497 | 1.6476 | 1.6433 | 69.7 | 66.2 | 72.2 | 73.5 |
| 11 | 1.6498 | 1.6460 | 1.6437 | 104.1 | 97.7* | 97.9** | |
| 12 | 1.6551 | 1.6572 | 1.6599 | 82.9 | 84.7 | 82.7 | |
| 13 | 1.6539 | 1.6551 | 1.6556 | 114.4 | 109.4 | 112.2 | |
| 14 | 1.6543 | 1.6581 | 1.6668 | 67.2 | 67.8 | 67.5 | |
| 15 | 1.6565 | 1.6597 | 1.6662 | 70.3 | 70.0 | 69.6 | |
| 16 | 1.6546 | 1.6589 | 1.6675 | 70.8 | 70.8 | 70.7 | |
| 17 | 1.6565 | 1.6609 | 1.6685 | 74.8 | 69.5 | 67.9 | |
| 18 | 1.6663 | 1.6753 | 1.6927 | 72.1 | 71.1 | 71.9 | |
| 19 | 1.6844 | 1.7124 | 1.7649 | 74.2 | 71.3 | 72.8 | |
| 20 | 1.7022 | 1.7273 | 1.7920 | 65.8 | 66.8 | 64.3 | |

*This value (and those below it) resulted from extinction measurements for wavelength 500nm.
**This value (and below it) resulted from extinction measurements at 540nm.

Table 6. Pleochroism and absorption formulae

| sample | $n_a$ | $n_b$ | $n_c$ | abs |
|---|---|---|---|---|
| 1 | colorless | colorless | very light reddish-pink | $n_a < n_b < n_c$ |
| 2 | colorless | colorless | light reddish-pink | $n_a < n_b < n_c$ |
| 3 | colorless | colorless | very light reddish-pink | $n_a < n_b < n_c$ |
| 4 | colorless | colorless | light reddish-pink | $n_a < n_b < n_c$ |
| 5 | colorless | colorless | light reddish-pink | $n_a < n_b < n_c$ |
| 6 | colorless | colorless | reddish-pink | $n_a < n_b < n_c$ |
| 7 | colorless | colorless | colorless | $n_a < n_b < n_c$ |
| 8 | colorless | colorless | colorless | $n_a < n_b < n_c$ |
| 9 | colorless | colorless | very light reddish-pink | $n_a < n_b < n_c$ |
| 10 | colorless | colorless | very light reddish-pink | $n_a < n_b < n_c$ |
| 11 | greenish-yellow | irish-greeen | golden-vellow | $n_a < n_b < n_c$ |
| 12 | very light yellow | light emerald-green | light golden-yellow | $n_a < n_b < n_c$ |
| 13 | light green-yellow | light emerald-green | light golden-yellow | $n_a < n_b < n_c$ |
| 14 | light yellow-green | emerald-green | golden-yellow | $n_a < n_c < n_b$ |
| 15 | light yellow | light emerald-green | light golden-yellow | $n_a < n_b = n_c$ |
| 16 | light yellow-green | emerald-green | golden-yellow | $n_a < n_c < n_b$ |
| 17 | greenish-yellow | emerald-green | golden-yellow | $n_a < n_c < n_b$ |
| 18 | yellowish-green | emerald-green | golden-yellow | $n_a < n_c < n_b$ |
| 19 | yellowish-green | emerald-green | golden-yellow | $n_a < n_c < n_b$ |
| 20 | green | deep emerald-green | deep golden-yellow | $n_a < n_c < n_b$ |

### *Lattice parameters*

The unit cell edges and volume are best predicted from (and related to) composition by equations 1, 3, 5 and 7 if $[x + y] > 0.05$, but by 1a, 3a, 5a and 7a if $[x + y] < 0.05$. Comparison of the coefficients for $x$ and $y$ in equations 1, 3 and 5 suggests that cell edge $a$ (and less so $b$) increases more with $Mn^{3+}$ content than with $Fe^{3+}$ content whereas for $c$ the reverse is markedly true. These dimensional changes in the unit cell appear to stem largely from the dimensional changes in the M(1) octahedra when occupied by $Mn^{3+}$ and $Fe^{3+}$. These octahedra, if occupied by $Mn^{3+}$, undergo a Jahn–Teller distortion which, as shown by Abs-Wurmbach *et al.* (1981) and by Weiss *et al.* (1981), increases the M(1)–O(4) distance by 0.16Å from andalusite to a kanonaite for which Abs-Wurmbach *et al.* report $x = 0.68$ and $y = 0.02$ whereas Vrana *et al.* report $x = 0.76$ and $y = 0.02$. Because the M(1)–O(4) vector aligns *(ca.)* at 30° to **a**, 60° to **b**, and 90° to **c**, $Mn^{3+}$ substitution hence increases cell edge $a$ most, cell edge $b$ less, and cell edge $c$ least of all. On the other hand, judging from the relative values for the coefficients for $y$ in equations 1, 3 and 5, $Fe^{3+}$ enlarges the M(1) octahedra without producing the distortion along M(1)–O(4).

Equations combining $x$ and $y$ into a single independent variable $[x + y]$ are at risk if $x$ and $y$ have significantly different effects on the independent variable. In this respect, the coefficients for $x$ and $y$ appear similar in value in equations 1 and 3, but not in equation 5. Not surprisingly, therefore, cell edges $a$ and $b$ also bear a fairly linear relationship to $[x + y]$, *cf.* equations 2 and 4, but $c$ does not. For $c$, a higher order equation (Equation 6) fits the data significantly better than the linear one. Aside from the slightly nonlinear relationship we report for $c$, the relationship of cell edges to $[x + y]$ observed by us corroborate those reached by Abs-Wurmbach *et al.* (1981) who studied four viridines, one kanonaite, and two synthetic viridines (Fig. 2). The decreasing slope of the curve for $c$, as high values of $[x + y]$ are approached, results because in our samples $x$ dominates over $y$ at high values of $[x + y]$ and less effectively increases $c$ (*cf.* Equation 5).

### *Optical properties*

Regressions were performed using successively, as the single dependent variable, $n_a$, $n_b$ and $n_c$, respectively the refractive indices for sodium light vibrating parallel to the $a$, $b$ and $c$ crystallographic axes. With $x$ and $y$ treated as separate independent variables, the models obtained from the full set of data (Table 8: Eqs. 9, 11, 13) indicate that each index increases more in response to $Fe^{3+}$ substitution than to $Mn^{3+}$ substitution. The models obtained using only the data for the 11 andalusites (Eqs. 9a, 11a, 13a) do not show this because only two of these 11 specimens contained appreciable $Mn^{3+}$. With $x$ and $y$ combined into the single

Table 7. Regression-derived models that relate unit cell parameters (in Å or Å$^3$) to $x$ and $y$ or $[x + y]$

| Eq. | REGRESSION MODEL OBTAINED | $R^2$ |
|---|---|---|
| | Range: full | |
| 1 | $a = 7.7908(13) + 0.258(6)x + 0.162(39)y$ | .993 |
| 2 | $a = 7.7887(10) + 0.253(6)[x+y]$ | .991 |
| 3 | $b = 7.8956(8) + 0.232(4)x + 0.191(25)y$ | .997 |
| 4 | $b = 7.8948(6) + 0.230(4)[x+y]$ | .996 |
| 5 | $c = 5.5529(4) + 0.091(2)x + 0.230(12)y$ | .996 |
| 6 | $c = 5.5538(6) + 0.148(9)[x+y] - 0.086(14)[x+y]^2$ | .989 |
| 7 | $V = 341.58(11) + 27.5(5)x + 29.2(32)y$ | .996 |
| 8 | $V = 341.68(8) + 27.6(4)[x+y]$ | .996 |
| | Range: $[x+y] < 0.05$ | |
| 1a | $a = 7.7923(3) + 0.268(21)x + 0.086(17)y$ | .958 |
| 2a | $a = 7.7918(7) + 0.155(32)[x+y]$ | .716 |
| 3a | $b = 7.8965(2) + 0.213(14)x + 0.168(14)y$ | .984 |
| 4a | $b = 7.8963(2) + 0.185(11)[x+y]$ | .970 |
| 5a | $c = 5.5534(4) + 0.050(28)x + 0.190(22)y$ | .905 |
| 6a | $c = 5.5538(6) + 0.137(28)[x+y]$ | .721 |
| 7a | $V = 341.71(4) + 24.1(27)x + 22.6(21)y$ | .961 |
| 8a | $V = 341.71(4) + 23.2(16)[x+y]$ | .960 |

Table 8. Regression-derived models that relate refractive indices to $x$ and $y$ or $[x + y]$

| Eq. | REFRACTIVE INDICES, BEST REGRESSION MODELS | $R^2$ |
|---|---|---|
| | Range: full | |
| 9 | $n_a = 1.6436(4) + 0.091(2)x + 0.158(11)y$ | .996 |
| 10 | $n_a = 1.6440(3) + 0.120(5)[x+y] - 0.046(8)[x+y]^2$ | .996 |
| 11 | $n_b = 1.6371(8) + 0.141(3)x + 0.331(24)y$ | .993 |
| 12 | $n_b = 1.6389(4) + 0.18(1)[x+y] + 0.12(5)[x+y]^2 - 0.30(6)[x+y]^3$ | .998 |
| 13 | $n_c = 1.6289(19) + 0.260(8)x + 0.524(57)y$ | .988 |
| 14 | $n_c = 1.6324(8) + 0.27(2)[x+y] + 0.47(9)[x+y]^2 - 0.8(1)[x+y]^3$ | .998 |
| | Range: $[x+y] < 0.05$ | |
| 9a | $n_a = 1.6436(4) + 0.132(26)x + 0.149(20)y$ | .910 |
| 10a | $n_a = 1.6436(3) + 0.142(15)[x+y]$ | .907 |
| 11a | $n_b = 1.6383(2) + 0.144(17)x + 0.210(13)y$ | .976 |
| 12a | $n_b = 1.6388(3) + 0.185(15)[x+y]$ | .947 |
| 13a | $n_c = 1.6328(3) + 0.236(22)x + 0.239(17)y$ | .975 |
| 14a | $n_c = 1.6328(3) + 0.238(13)[x+y]$ | .975 |

independent variable $[x + y]$, higher order terms in $[x + y]$ become significant in the models derived from the full set of data (Eqs. 10, 12 and 14).

A plot of the refractive index data and of Equations 10, 12 and 14 (Fig. 3) illustrates that all three curves intersect at or near $[x + y] = 0.066$. This also held true for curves relating the refractive indices for wavelength 486.1 nm (and for 656.3 nm) to $[x + y]$. In this region, therefore, andalusite becomes nearly isotropic. The lack of specimens in this region, as evidenced by the gap between crystals 11 and 12 (Fig. 3), possibly arises from failure to recognize andalusite in this near-isotropic form.

It is proper to plot the refractive indices $n_a$, $n_b$ and $n_c$ against $[x + y]$ as the single independent variable only to the extent that $Fe^{3+}$ and $Mn^{3+}$ have identical effects on each of these indices. As already noted, however, Equations 9, 11 and 13 indicate that $Fe^{3+}$ causes a greater increase in $n_a$, $n_b$ and $n_c$ than does $Mn^{3+}$. Indeed these equations are much to be preferred over Equations 10, 12 and 14, if composition is to be used to predict refractive index. The downward slope that Equations 10, 12 and 14 display at high values of $[x + y]$ in Figure 3 results because (1) $Mn^{3+}$ content dominates over $Fe^{3+}$ content in crystals 14 to 20 (and especially 18–20) and, as noted, (2) $Mn^{3+}$ increases the refractive indices less effectively than $Fe^{3+}$. The indices for crystals containing high amounts of $Fe^{3+}$ will likely plot above the curves in Figure 3.

Before the crystal structures of andalusite and "viridine" were known, Wülfing (1917) concluded they were different mineral species because of their differing optical orientations—$X = c$, $Y = b$, $Z = a$

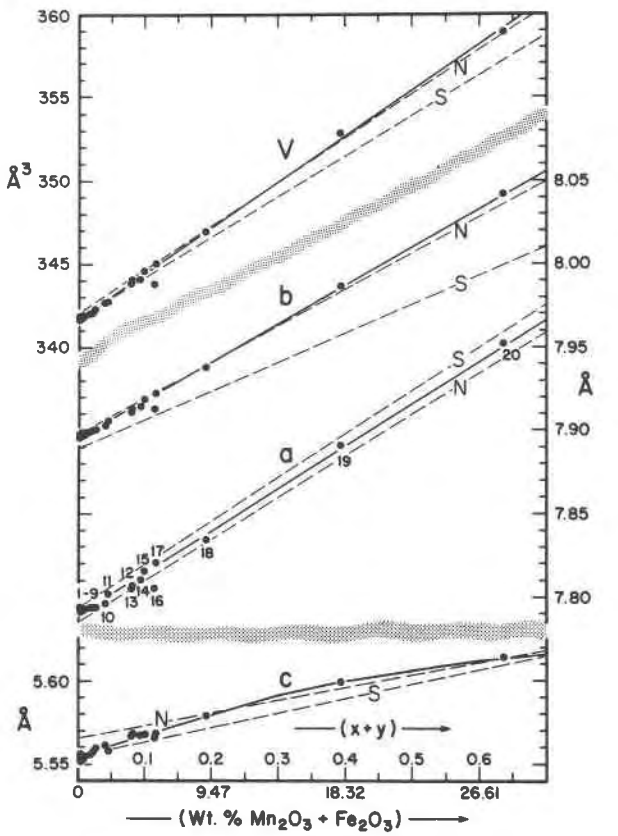


Fig. 2. Cell edges and volume *vs.* $[x + y]$. The trend lines represent Equations 2, 4, 6 and 8 (Table 7) and compare to those (=dashed lines) obtained by Abs-Wurmbach *et al.* (1981) for natural (N) and synthetic (S) andalusites and viridines. The downward curvature shown for $c$ as $[x + y]$ increases (Eq. 6) results because $Mn^{3+}$, which dominates increasingly over $Fe^{3+}$ from crystals 14 to 20, increases $c$ less effectively than $Fe^{3+}$ (*cf.* Equation 5). For crystal compositions given as weight percent $Mn_2O_3$ and $Fe_2O_3$, if $W_{MF}$ represents the sum of these two weight percents, then $[x + y]$ can be readily calculated from

$$[x + y] = \left(\frac{49.0}{W_{MF}} - 0.175\right)^{-1}$$

This equation derives from the more general one

$$[x + y] = \frac{2\,(M_S + M_A)\,W_{MF}}{100\,M_{MF} - (M_{MF} - M_A)\,W_{MF}}$$

where $M_S$ $M_A$ and $M_{MF}$ respectively represent the molecular weights of $SiO_2$, $Al_2O_3$, and the average for $Mn_2O_3$ and $Fe_2O_3$. Both equations were kindly derived by Mr. Shu-Chun Su and are approximate to the extent that $M_{MF}$ differs from the actual molecular weights for $Mn_2O_3$ and $Fe_2O_3$. The scale is non-linear for $W_{MF}$. For example, $W_{MF}$ values 9.47, 18.32 and 26.61 respectively plot at the points where the linear $[x + y]$ scale equals 0.2, 0.4 and 0.6.

(andalusite) and $X = a$, $Y = b$, $Z = c$ ("viridine")—which caused {110} cleavage prisms to be length-fast for andalusite but length-slow for "viridine". Subsequent crystal structure analyses, however, disclosed the two to be isostructural and, as Figure 3 shows, this change in optical orientation is simply a compositional effect. Later authors have overlooked the difference in optical orientation between andalusite and viridine and have attempted to plot the indices $\alpha$, $\beta$ and $\gamma$ *versus* $[x + y]$. So plotted, the curve for $\alpha$ is then a segment of $n_c$ (for $[x + y] < 0.066$) joined to one of $n_a$ (for $[x + y] > 0.066$). The $\gamma$ curve is a similar amalgam.

With increase in $[x + y]$, the rate of cell-edge increase is $dc < db < da$ (Fig. 2) whereas, somewhat inversely, the refractive indices increase at rates $dn_c > dn_b > dn_a$ (Fig. 3). The faster rate of increase of $n_c$ relative to $n_a$ results because $Mn^{3+}$ and $Fe^{3+}$ largely substitute for $Al^{3+}$ in the M(1) sites—that is, in the edge-sharing octahedral chains parallel to $c$ in andalusite. As Equation 5 (Table 7) illustrates, these chains resist lengthening along $c$ as $Mn^{3+}$ (but not $Fe^{3+}$) substitutes for the smaller $Al^{3+}$. Perpendicular to the chain, however, as Weiss *et al.* (1981) document, a marked lengthening of the M(1)–O(4) bond, from 2.085Å (andalusite) to 2.242Å (kanonaite), occurs with $Mn^{3+}$ substitution. This pronounced Jahn–Teller bipyramidal distortion of the M(1) octahedra in kanonaite, also observed by Abs-Wurmbach *et al.* (1981), likely decreases the ability of the M(1) occupant to distort (polarize) the electron cloud about O(4) along the M(1)–O(4) direction. Consequently, as $Mn^{3+}$ (and $Fe^{3+}$?) enters the M(1) sites, increase in the refractive index is opposed for those principal vibrations most nearly parallel to the M(1)–O(4) bond. Hence, the slope in Figure 3, at $[x + y] < 0.4$, is least for $n_a$ (the $a$-axis being at ~30° to this bond), somewhat more for $n_b$ ($b$ being at ~60°), and most for $n_c$ ($c$ being at ~90°). Weiss *et al.* (1981) observe that even Mn-free specimens display a Jahn–Teller-like distortion of the M(1) octahedra.

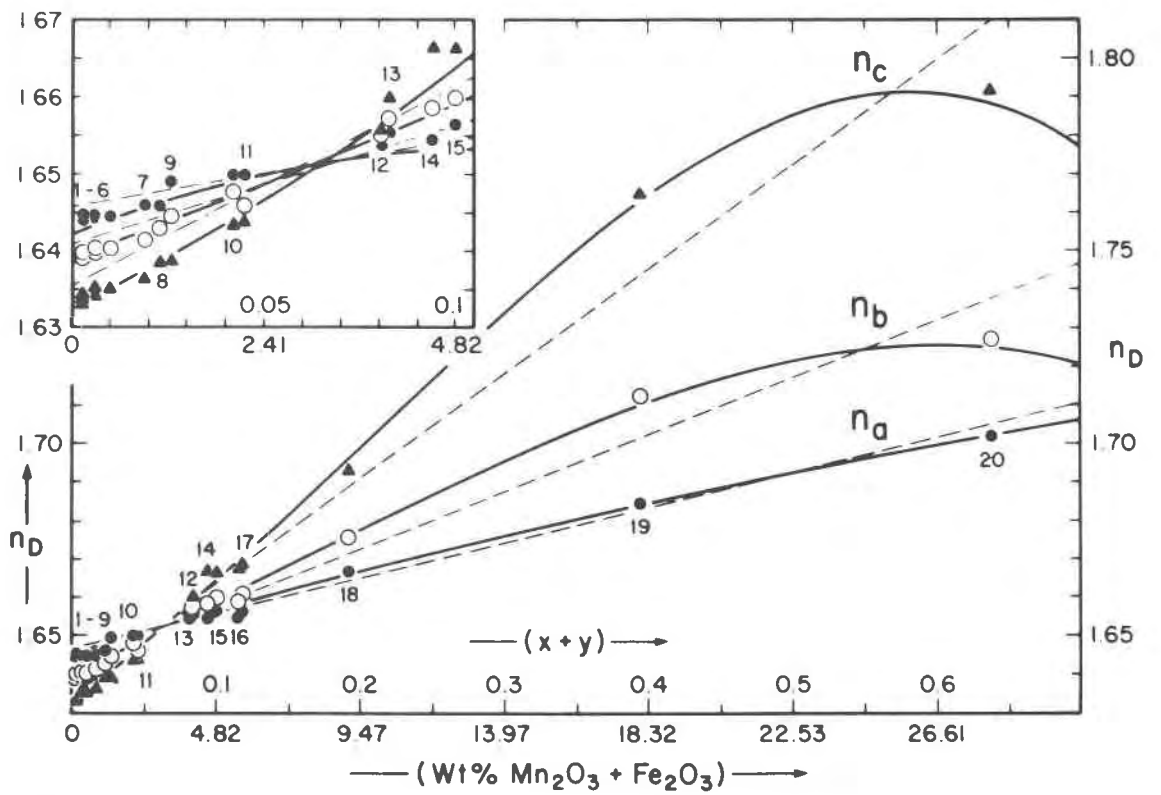


Fig. 3. Refractive indices for sodium light vibrating parallel to the $a$-axis ($n_a$), $b$-axis ($n_b$) and $c$-axis ($n_c$) *vs.* $[x + y]$. As $[x + y]$ increases, the solid trend lines (Equations 10, 12, 14 in Table 8) curve downward below the linear fits (dashed lines) because $Mn^{3+}$ dominates increasingly over $Fe^{3+}$ in crystals 14 to 20 and less effectively increases their indices, especially for $n_b$ and $n_c$. (*cf.* the extent to which the coefficient for $y$ exceeds that for $x$ in Equations 9, 11 and 13 in Table 8). The upper left inset represents an enlarged drawing for andalusites with $[x + y]$ less than 0.1.

Lengthening of the M(1)–O(1) and M(1)–O(2) bonds with $Mn^{3+}$ substitution is considerably less than for M(1)–O(4). Weiss *et al.* (1981) observed M(1)–O(1) to change from 1.829Å (andalusite) to 1.850Å (kanonaite) and M(1)–O(2) to change from 1.892Å (andalusite) to 1.916Å (kanonaite). These increases in bond lengths, being roughly one-tenth that for M(1)–O(4), presumably less importantly affect the rate of refractive index increase for andalusite as $Mn^{3+}$ enters its structure.

In common with other compendia of optical properties, Bambauer *et al.* (Troger, 1979) report that, for andalusite, $(\gamma - \alpha)$ ranges from 0.009 to 0.011. For our specimen 11, which contained the most $Mn^{3+}$ and $Fe^{3+}$ of the eleven andalusites studied, $(\gamma - \alpha)$ for sodium light equals 0.006 (Table 5). For viridines, Bambauer *et al.* report $(\gamma - \alpha)$ to range from 0.013 to 0.029. On the other hand, for our specimen 13, which on basis of optical orientation is a "viridine" (or manganian–ferrian andalusite), $(\gamma - \alpha)$ seems less than 0.002.

For $2V_c$, the optic angle measured around the $c$ axis, values were calculated from the principal indices for sodium light (Table 5). Independent values of $2V_c$ were also obtained by the extinction method of Bloss and Riess (1973) with the extinction data being processed by EXCALIBR (Bloss, 1981). For crystals 1 to 9, extinction measurements were made—and $2V_c$ determined—at wavelengths 400, 666, and 900 nm (Table 5). Crystals 11 to 20, however, were insufficiently transparent except between 500–540 nm. For these crystals, accordingly, extinctions were measured and $2V_c$ calculated only for wavelengths 500 and 540 nm.

Attempts to correlate $2V_c$ with composition failed. Reasons for this could be (1) non-recognition of a factor significantly affecting $2V_c$ or (2) marked variations in $2V_c$ in response to minor changes in composition for crystals with low values of $(\gamma - \alpha)$ such as specimens 10, 11, 12 and 13 (Fig. 3).

*Pleochroism and absorption*

The pleochroic colors associated with light vibrating parallel to the $a$, $b$ and $c$ axes in andalusite are summarized in Table 6. Curiously, crystal 11, which is on the andalusite side of the intersection of the curves for $n_a$ and $n_c$ (Fig. 3), possesses a pleochroism more akin to that of the "viridines". $2V_c$ is anomalously high for crystal 11, although not so high as for crystal 13, which displays similar pleochroism and absorption. A compositional factor other than substitution of $Mn^{3+}$ and $Fe^{3+}$ in the M(1) site may possibly be involved.

*Properties of pure andalusite*

Equations 1a, 3a, 5a, 7a, 9a, 11a, and 13a resulted from regressions performed on only the data for the 11 specimens (andalusites) for which $[x + y] < 0.05$. Their intercepts, in consequence, represent a very small extrapolation beyond the range of the data points. Accordingly, we accept these intercepts as the best estimates for the cell edges, cell volume, and refractive indices for pure andalusite ($x = y = 0$). Interestingly, the nonlinear models relating refractive indices to $[x + y]$ for the full set of data (Eqs. 10, 12 and 14) had intercepts statistically indistinguishable from those for Eqs. 9a, 11a, and 13a.

For pure andalusite, therefore, we suggest that $a = 7.7923(3)$, $b = 7.8965(2)$, $c = 5.5534(4)$Å, $V = 341.71(4)$Å$^3$ and that, by calculation, its density equals 3.149 g cm$^{-3}$ and its molar volume 51.45(4) cm$^3$. For comparison, Robie and Waldbaum (1968) cite andalusite's molar volume to be 51.53(4) cm$^3$. Its refractive indices for sodium light are likely to be 1.6328(3), 1.6386(2), and 1.6436(4), for which $2V_x$ calculates to be 85.5°, or the statistically identical values (from Eqs. 10, 12 and 14) 1.6324(8), 1.6389(4) and 1.6440(3) for which $2V_x$ calculates to be 82.8°. Textbooks, probably following Ellsworth and Jolliffe (1937), commonly cite the indices for andalusite as 1.629, 1.633 and 1.638. These are patently incorrect. They are the indices for a (+) crystal whereas, as even these textbooks note, andalusite is (−). Better values were determined by Hietanen (1956) who obtained 1.631(1), 1.637(1) and 1.642(1) for one specimen and 1.631(1), 1.638(1), and 1.643(1) for a second. Rather ironically, the values reported by Taubert (1905)—namely, 1.6326, 1.6390 and 1.6440—have been overlooked by most mineralogists and petrologists.

*Andalusite as a mineral name*

The question remains as to how pure natural andalusite must be to be called, simply, andalusite. We here suggest that the term andalusite, unmodified, be restricted to andalusites which display (−) or length-fast elongations relative to the {110} cleavage. This restricts the name to specimens with the orientation $a = Z$, $b = Y$, $c = X$ and thus to specimens for which, approximately, $[x + y] < 0.066$. Specimens which display (+) or length-slow elongation relative to {110} will thus be either manganian andalusites, aluminous kanonaites, or "viridines" (ferrian manganian andalusites). This suggestion, submitted as a proposal to the IMA Commission, received 8 approving and 6 disapproving

votes hence falling short of the required 2/3 majority. Thus, by the Commission's rulings, some kanonitic andalusites will be length-fast relative to {110} but others will be length-slow. In view of this, the statement by most (if not all) optical mineralogy texts—that andalusite is length-fast but "viridine" length-slow—requires revision.

*Predictive equations*

From measured physical parameters it may sometimes be convenient to predict the value of $[x + y]$ for a member of the andalusite–kanonaite series. Thus, if the principal refractive indices for sodium light are known, the following model

$$[x + y] = -12.47 + 15.00295n_a - 13.19163n_b + 5.77439n_c$$

will generally predict $[x + y]$ to (*ca.*) 0.01. The model can also be used unconventionally to predict, if $x$ and $y$ are known, whether $n_c = \alpha$ and $n_a = \gamma$—or *vice versa*. Presumably, the model's right-hand side will more closely equal $x + y$ if the correct optic orientation is chosen.

Using the unit cell volume in cubic angstroms, the model

$$[x + y] = -12.348 + 0.03615\ V$$

will usually predict $[x + y]$ to within 0.02.

The multiple linear regressions provided no models that permitted satisfactory prediction of individual values of $x$ or $y$.

## Acknowledgments

We are grateful to the State of Virginia for Grant number G5106007 from the Mining and Mineral Resource and Research Institute which made this work possible. Professors G. V. Gibbs and Paul H. Ribbe kindly read the paper and offered helpful suggestions. At Virginia Polytechnic Institute, Jim Light, Don Bodell, and Todd Solberg provided outstanding technical assistance in support of the project. At the University of New Mexico, George Conrad helped with microprobe analyses and the Caswell Silver Foundation, by support of one of us (F.D.B), aided in preparation of the manuscript. We thank Drs. John S. White of the Smithsonian Institution, Edward Olsen of the Field Museum of Natural History, and I. Abs-Wurmbach of the University of Bern for providing the samples studied. Dr. I. Abs-Wurmbach's review of the manuscript was particularly valuable. We are grateful to Dr. Thomas Armbruster, also of the University of Bern, for his help and suggestions throughout the course of this work.

## References

Abs-Wurmbach, I., Langer, K., Seifert, F., and Tillmanns, E. (1981) The crystal chemistry of ($Mn^{3+}$, $Fe^{3+}$)-substituted andalusites (viridines and kanonaite) $(Al_{1-x-y}Mn_x^{3+}Fe_y^{3+})_2(O|SiO_4)$: crystal structure refinements, Mössbauer, and polarized optical absorption spectra. Zeitschrift für Kristallographie, 155, 81–113.

Bäckström, H. (1896) Manganandalusite von Vestana. Geologiska Forenigens i Stockholm Forhandlungen, 18, 386–389.

Bloss, F. D. (1981) The spindle stage: principles and practice. Cambridge University Press, Cambridge and New York.

Bloss, F. D. and Riess, D. (1973) Computer determination of $2V$ and indicatrix orientation from extinction data. American Mineralogist, 58, 1052–1061.

Buerger, M. J. (1937) The precision determination of the linear and angular lattice constants of single crystals. Zeitschrift für Kristallographie, 97, 433–468.

Burnham, C. W. (1962) Lattice constant refinement. Carnegie Institution of Washington Year Book, 61, 132–135.

Burnham, C. W. (1965) Refinement of lattice parameters using systematic correction terms. Carnegie Institution of Washington Year Book, 64, 200–202.

Burnham, C. W. and Buerger M. J. (1961) Refinement of the crystal structure of andalusite. Zeitschrift für Kristallographie, 115, 269–290.

Deer, W. A., Howie, R. A., and Zussman, J. (1966) An Introduction to the Rock Forming Minerals. Longman Group Limited, London.

Ellsworth, H. V. and Jolliffe, F. (1937) Some recently-discovered minerals of the Great Slave Lake area, N. W. T. University of Toronto Studies Geological Series, No. 40, 71–81.

Finger, L. W. and Prince, E. (1971) Neutron diffraction studies: anadalusite and sillimanite. Carnegie Institution of Washington Year Book, 70, 496–500.

Helwig, J. T. and Council, K. A. (1979) SAS User's Guide 1979 Edition. SAS Institute Inc., Cary, North Carolina, 27511.

Herbosch, A. (1968) La viridine et la braunite de Salm Chateau. Bulletin Société Géologie Belgique, 76, 183–204.

Hietanen, Anna (1956) Kyanite, andalusite, and sillimanite in the schist in Boehls Butte quadrangle, Idaho. American Mineralogist, 41, 1–19.

Holdaway, M. J. (1971) Stability of andalusite and the aluminum silicate phase diagram. American Journal of Science, 271, 97–131.

Klemm, G. (1911) Über Viridin. eine Abart des Andalusites. Notizblatt Verein für Erdkunde, Darmstadt, 32, 4–13.

Louisnathan, S. J., Bloss, F. D., and Korda, E. J. (1978) Measurement of refractive indices and their dispersion. American Mineralogist, 63, 394–400.

Peterson, R. C. and McMullen, R. K. (1980) Neutron structure refinements of the $Al_2SiO_5$ polymorphs. Transactions of the American Geophysical Union, EOS 61, 409.

Robie, R. A. and Waldbaum, D. R. (1968) Thermodynamic properties of minerals and related substances at 298.15°K (25.0°C) and one atmosphere (1.013 bars) pressure and at higher temperatures. U. S. Geological Survey, Bulletin 1259.

Schneider, Hartmut (1979) Thermal expansion of andalusite. Journal of the American Ceramic Society, 62, 5–6.

Skinner, B. J., Clark, S. P. Jr., and Appleman, D. E. (1961) Molar volumes and thermal expansions of andalusite, kyanite, and sillimanite. American Journal of Science, 259, 651–668.

Strens, R. G. J. (1968) Stability of $Al_2SiO_5$ solid solutions. Mineralogical Magazine, 36, 839–849.

Taubert, (1905) Dissert. Jena. as cited by Landolt, H. H. and Börnstein, R. (1962) in Zahlenwerte und Funktionen aus Physik, Chemie, Astronomie, vol. II, Teil 8: Optische Konstanten. Springer Verlag, Berlin, Heidelberg, and New York.

Taylor, W. H. (1929) The structure of andalusite, $Al_2SiO_5$. Zeitschrift für Kristallographie, 71, 205–218.

Tröger, W. E. (1979) Optical determination of rock-forming minerals (by Bambauer, H. U., Taborszky, F. and Trochim, H. D.) E. Schweizerbart'sche Verlagsbuchhandlung, Stuttgart.

Vrana, S. M., Rieder, M. and Podlaha, J. (1978) Kanonaite $(Mn_{0.76}Al_{0.23}Fe_{0.02})$ Al O $SiO_4$, a new mineral isotypic with andalusite. Contributions to Mineralogy and Petrology, 66, 325–332.

Weiss, Z., Bailey, S. W., and Rieder, M. (1981) Refinement of the crystal structure of kanonaite, $(Mn^{3+}, Al)^{[6]}$ $(Al, Mn^{3+})^{[5]}$ O $[SiO_4^-]$. American Mineralogist, 66, 561–567.

Winter, J. K. and Ghose, Subrata, (1979) Thermal expansion and high-temperature crystal chemistry of the $Al_2SiO_5$ polymorphs. American Mineralogist, 64, 573–586.

Wülfing, E. A. (1917) Der Viridin und seine Beziehung zum Andalusit. Sitzungsberichte der Heidelberger Akademie der Wissenschaften, Matematisch–Naturwissenschaftliche Klasse, Abteilung A.

*Manuscript received, December 28, 1981; accepted for publication, July 6, 1982.*